

Statistical mechanics and phase diagrams of rotating self-gravitating fermions

P.H. Chavanis¹ and M. Rieutord^{2,3}

¹ Laboratoire de Physique Théorique, Université Paul Sabatier, 118 route de Narbonne 31062 Toulouse, France
e-mail: chavanis@irsamc.ups-tlse.fr

² Observatoire Midi-Pyrénées, 14 av. E. Belin, F-31400 Toulouse, France

³ Institut Universitaire de France
e-mail: rieutord@ast.obs-mip.fr

February 7, 2020

Abstract. We compute statistical equilibrium states of rotating self-gravitating systems enclosed within a box by maximizing the Fermi-Dirac entropy at fixed mass, energy and angular momentum. The Fermi-Dirac distribution describes quantum particles (fermions) subject to Pauli's exclusion principle. It is also a typical prediction of Lynden-Bell's theory of violent relaxation for collisionless stellar systems (in that case degeneracy accounts for the Liouville theorem). We increase the rotation up to the Keplerian limit and describe the flattening of the configuration until mass shedding occurs. At the maximum rotation, the system develops a cusp at the equator. We draw the equilibrium phase diagram of the rotating self-gravitating Fermi gas and discuss the structure of the caloric curve as a function of degeneracy parameter and angular velocity. We argue that systems described by the Fermi-Dirac distribution in phase space do not bifurcate to non-axisymmetric structures, in continuity with the case of polytropes with index $n > 0.808$ (the Fermi gas at $T = 0$ corresponds to $n = 3/2$). This contrasts with the study of Votyakov et al. (2002) who consider a Fermi-Dirac distribution in configuration space and find "double star" structures (their model at $T = 0$ corresponds to $n = 0$). We also discuss the influence of rotation on the onset of the gravothermal catastrophe for globular clusters. On general grounds, we complete previous investigations concerning the nature of phase transitions in self-gravitating systems. We emphasize the inequivalence of statistical ensembles regarding the formation of binaries (or low-mass condensates) in the microcanonical ensemble and Dirac peaks (or massive condensates) in the canonical ensemble. We also describe an *hysteretic cycle* between the gaseous phase and the condensed phase that are connected by a "collapse" or an "explosion". This notion of hysteresis in self-gravitating systems is new.

Key words. Stellar dynamics-hydrodynamics, instabilities

1. Introduction

It is striking to observe that self-gravitating systems follow a kind of organization despite the diversity of their initial conditions and their environment. This organization is illustrated by morphological classification schemes such as the Hubble sequence for galaxies and by simple rules which govern the structure of individual self-gravitating systems. For example, elliptical galaxies display a quasi-universal luminosity profile described by de Vaucouleur's $R^{1/4}$ law and most of globular clusters are well-fitted by the Michie-King model. On the other hand, the rotation curves of spiral galaxies appear to be flat and this striking observation can be explained by the presence of a dark matter halo with a density profile decreasing as r^{-2} at large distances (Binney & Tremaine 1987).

The question that naturally emerges is what determines the particular configuration to which a self-gravitating system settles. It is possible that their actual configuration crucially depends on the conditions that prevail at their birth and on the details of their evolution. However, in view of their apparent regularity, it is tempting to investigate whether their organization can be favoured by some fundamental physical principles like those of thermodynamics and statistical physics. We ask therefore if the actual states of self-gravitating systems are not simply more probable than any other possible configuration, i.e. if they cannot be considered as *maximum entropy states* (Chavanis 2002a).

This thermodynamical approach may be particularly relevant for globular clusters and elliptical galaxies whose distribution function is close to the isothermal one (at least in the inner region of the system). In the case of

globular clusters, the relaxation proceeds via two-body encounters and this collisional evolution is governed by the Fokker-Planck-Landau kinetic equation for which a H-theorem is available (see Kandrup 1981 for a precise discussion). This collisional evolution can lead to the establishment of a statistical equilibrium state. This equilibrium state is usually described by the Michie-King model, a truncated isothermal, which takes into account the escape of high energy stars due to tidal forces (Michie 1963, King 1966). In fact, such equilibria are only *metastable* (Antonov 1962) and the evolution continues for longer times with the formation of binaries (Hénon 1961). By contrast, for elliptical galaxies, two-body encounters are completely negligible (the corresponding relaxation time t_{coll} exceeds the age of the universe by many orders of magnitude) and the galaxy dynamics is described by the Vlasov equation, i.e. collisionless Boltzmann equation. Yet, collisionless stellar systems can reach a meta-equilibrium state as a result of a *violent relaxation* (Lynden-Bell 1967). The general prediction of the equilibrium state is complicated and depends on the initial conditions. Furthermore, the meta-equilibrium state actually reached by the system may differ from the statistical prediction due to *incomplete relaxation* (Lynden-Bell 1967). Therefore, generalized entropy functionals, called H -functions, must be constructed to account for the structure of elliptical galaxies (Tremaine, Hénon & Lynden-Bell 1987, Hjorth & Madsen 1993, Chavanis 2003a,c).

The thermodynamics of self-gravitating systems started with the discoveries by Emden (1907), Bonnor (1956) and Antonov (1962) that a self-gravitating isothermal gas can be in hydrostatic equilibrium only in a limited range of thermodynamical parameters (temperature, external pressure and energy). Outside this range, the thermodynamical potential (free energy, entropy or Gibbs energy) has no extremum and the system is expected to collapse under its own gravity (Lynden-Bell & Wood 1968, Chavanis 2003a). A “core-halo” phase halting the collapse can be evidenced if we introduce appropriate small-scale cut-offs. Different regularizations have been proposed such as quantum degeneracy, hard spheres, soften potential,... Then, the shape of the caloric curve $T(E)$ depends on an additional parameter μ related to the inverse of the small-scale cut-off (see Chavanis 2002b). For $\mu \rightarrow +\infty$, one recovers the classical results of Emden, Bonnor and Antonov. As the cut-off increases, it is possible to describe phase transitions between a “gaseous” phase (independant on the small-scale cut-off) and a “condensed” phase (independant on the large-scale truncation) with a core-halo structure. It is important to stress that the statistical ensembles are not interchangeable for self-gravitating systems (Padmanabhan 1990) and that phase transitions occur not only in the canonical ensemble but also in the microcanonical ensemble (Chavanis 2002b, Chavanis & Ispolatov 2002) which is a rather new phenomenon.

In the previous studies, the system is supposed to be non-rotating. The thermodynamics of rotating self-gravitating systems was studied by Lagoute & Longaretti

(1996) in the framework of Michie-King models describing globular clusters. The case of a slowly rotating isothermal gas confined within a spherical box was treated by Chavanis (2002c) using analytical methods introduced by Milne (1923) and Chandrasekhar (1933) for distorted polytropes. Recently, Votyakov et al. (2002) considered the thermodynamics of rapidly rotating self-gravitating systems and showed that phase transitions from axisymmetric to non-axisymmetric structures (“double stars”) occur at sufficiently high values of angular momentum. These authors provide an interesting phase diagram of rotating self-gravitating systems for arbitrary values of angular momentum and energy. However, the adopted distribution function corresponds to a Fermi-Dirac statistics in *configuration* space. This is at variance with the usual Fermi-Dirac distribution function in *phase* space which is valid for quantum particles due to Pauli’s exclusion principle (Chandrasekhar 1942) or for the violent relaxation of collisionless stellar systems (Chavanis & Sommeria 1998). In the latter, the statistical approach refers to a *coarse-graining* of the distribution function and the effective exclusion principle is a consequence of the Liouville theorem associated with the collisionless nature of the evolution (Lynden-Bell 1967, Chavanis 2002d).

The distinction between the distribution function used by Votyakov et al (2002) and the ordinary Fermi-Dirac distribution function in phase space is crucial when the system is rotating. At $T = 0$ (or $E = E_{min}$), the former leads to a *homogeneous* body ($\rho = \text{Cst.}$) while the latter leads to a polytrope with index $n = 3/2$ corresponding to a classical white dwarf star ($p = K\rho^{5/3}$). Now, it is well-known that a uniformly rotating homogeneous mass is axisymmetric (spheroidal) for slow rotations (Maclaurin sequence) but bifurcates to non-axisymmetric configurations at sufficiently high rotations (Chandrasekhar 1969). These non-axisymmetric structures are usually ellipsoidal (Jacobi sequence) but more complex structures (pear-shaped, dumbbell,...) have also been found. The fission of the self-gravitating fluid into a binary state is also possible (Hachisu & Eriguchi 1984) and these binary states appear in the study of Votyakov et al. (2002) at low temperatures and high rotations. On general grounds, the fission instability has been extensively discussed in relation with the formation of binary stars and with the formation of the moon (in the non-symmetrical case). However, the fission scenario may not be the relevant mechanism and it is almost abandoned at present. Binary stars are more likely to result from the fragmentation of the molecular cloud (Boss 1988) and the moon has probably been detached from the protoearth after a collision with a Mars-sized body (Boss 1986). In contrast to incompressible fluid masses, a polytropic configuration with index $n > 0.808$ does *not* bifurcate to non-axisymmetric structures when angular velocity is increased; it remains axisymmetric until the Keplerian limit is reached (James 1964). At that point there is mass shedding and disruption of the system. This concerns in particular polytropes of index $n = 3/2$ (white dwarfs) which are the zero temperature limit of the Fermi

distribution (Fowler 1926). Therefore, the phase diagram corresponding to the Fermi-Dirac statistics in phase space is expected to differ from the one calculated by Votyakov et al. (2002). In this paper, we propose to compute this phase diagram for arbitrary rotation and degeneracy parameter in both microcanonical and canonical ensembles. We shall restrict ourselves to axisymmetric configurations since only axisymmetric configurations are expected to be relevant in our problem. The present study completes the description of non-rotating or slowly rotating fermionic structures discussed previously (Chavanis 2002b,c).

2. Statistical mechanics of rotating self-gravitating systems

2.1. The maximum entropy state

Consider a system of N particles, each of mass m , interacting via Newtonian gravity. We allow the system to have a non-vanishing angular momentum. Let $f(\mathbf{r}, \mathbf{v}, t)$ denote the distribution function of the system, i.e. $f(\mathbf{r}, \mathbf{v}, t)d^3\mathbf{r}d^3\mathbf{v}$ gives the mass of particles whose position and velocity are in the cell $(\mathbf{r}, \mathbf{v}; \mathbf{r} + d^3\mathbf{r}, \mathbf{v} + d^3\mathbf{v})$ at time t . The integral of f over the velocity determines the spatial density

$$\rho = \int f d^3\mathbf{v}. \quad (1)$$

The mass and angular momentum of the configuration are given by

$$M = \int \rho d^3\mathbf{r}, \quad (2)$$

$$\mathbf{L} = \int f \mathbf{r} \times \mathbf{v} d^3\mathbf{r}d^3\mathbf{v}. \quad (3)$$

On the other hand, in the mean-field approximation, the energy can be expressed as

$$E = \frac{1}{2} \int f v^2 d^3\mathbf{r}d^3\mathbf{v} + \frac{1}{2} \int \rho \Phi d^3\mathbf{r} = K + W, \quad (4)$$

where K is the kinetic energy and W the potential energy. The gravitational potential Φ is related to the star density by the Newton-Poisson equation

$$\Delta\Phi = 4\pi G\rho. \quad (5)$$

On general grounds, an interesting problem is to determine equilibrium configurations of stellar systems which maximize a H -function

$$S = - \int C(f) d^3\mathbf{r}d^3\mathbf{v}, \quad (6)$$

at fixed mass, energy and angular momentum, where $C(f)$ is a convex function, i.e. $C''(f) > 0$ (Tremaine et al. 1987, Chavanis 2003a,c). For collisional stellar systems (e.g., globular clusters), statistical mechanics predicts that S is the Boltzmann entropy (Ogorodnikov 1965)

$$S = - \int f \ln f d^3\mathbf{r}d^3\mathbf{v}. \quad (7)$$

For collisionless stellar systems experiencing violent relaxation, the prediction of $C(f)$ is less straightforward and depends on the initial conditions (Lynden-Bell 1967). In addition, because of incomplete relaxation, the function $C(f)$ may differ from the statistical prediction (e.g., Hjorth & Madsen 1993). In any case, the maximization of a H -function $S[f]$ at fixed M , E and \mathbf{L} determines a nonlinearly stable stationary solution of the Vlasov-Poisson system (Ipser & Horwitz 1979). It has also been suggested (Chavanis 2003a) that partially relaxed stellar models can be constructed by maximizing a H -function with the usual constraints and additional adiabatic invariants like $\mathbf{L}_2 = \int f(\mathbf{r} \times \mathbf{v})^2 d^3\mathbf{r}d^3\mathbf{v}$ for example.

In the following, we shall consider the Fermi-Dirac entropy

$$S = - \int \left\{ \frac{f}{\eta_0} \ln \frac{f}{\eta_0} + \left(1 - \frac{f}{\eta_0}\right) \ln \left(1 - \frac{f}{\eta_0}\right) \right\} d^3\mathbf{r}d^3\mathbf{v}, \quad (8)$$

as a typical prediction of Lynden-Bell's theory of violent relaxation. It corresponds to the two-levels approximation of his theory, $f_0 = 0$ or $f_0 = \eta_0$, where f_0 is the initial distribution function (Chavanis & Sommeria 1998). The Fermi-Dirac entropy (8) also describes a system of self-gravitating fermions (electrons or neutrons in white dwarf and neutron stars, massive neutrinos in dark matter models...) in which case $\eta_0 = (2s+1)m^4/(2\pi\hbar)^3$ is the maximum allowable value of the distribution function fixed by Pauli's exclusion principle (s is the spin). In the non degenerate limit $f \ll \eta_0$, we recover the Boltzmann entropy (7) of globular clusters as a special case. Therefore, the Fermi-Dirac entropy offers an interesting model of self-gravitating systems with several astrophysical applications.

Looking for critical points of entropy at fixed mass, energy and angular momentum and introducing Lagrange multipliers α , β and $-\beta\Omega$ for each constraint, we obtain the Fermi-Dirac distribution function

$$f = \frac{\eta_0}{1 + \lambda e^{\beta(\epsilon - \Omega \cdot \mathbf{j})}}, \quad (9)$$

where $\epsilon = \frac{w^2}{2} + \Phi$ and $\mathbf{j} = \mathbf{r} \times \mathbf{v}$ are the energy and the angular momentum of a star by unit of mass and $\beta = 1/T$ is the inverse temperature (we include m or η_0 in the definition of T). Introducing the Jacobi energy $\epsilon_J \equiv \epsilon - \Omega \cdot \mathbf{j}$ and noting that $\epsilon_J = \frac{w^2}{2} + \Phi_{eff}$, where $\mathbf{w} = \mathbf{v} - \Omega \times \mathbf{r}$ is the relative velocity and $\Phi_{eff} = \Phi - \frac{1}{2}(\Omega \times \mathbf{r})^2$ is the effective potential accounting for inertial forces, we can rewrite Eq. (9) in the form

$$f = \frac{\eta_0}{1 + \lambda e^{\beta(\frac{w^2}{2} + \Phi_{eff})}}. \quad (10)$$

We note that the “most probable” form of rotation is a rigid rotation Ω . The gravitational potential Φ is defined within an arbitrary gauge constant. We shall take the ordinary convention $\Phi \rightarrow 0$ at infinity.

By integrating Eq. (10) over the velocity, we find that the density is given by

$$\rho = \frac{4\pi\sqrt{2}\eta_0}{\beta^{3/2}} I_{1/2}(\lambda e^{\beta\Phi_{eff}}), \quad (11)$$

where I_n is the Fermi integral

$$I_n(t) = \int_0^{+\infty} \frac{x^n}{1+te^x} dx. \quad (12)$$

The equilibrium configuration is then obtained by solving the Fermi-Poisson equation

$$\Delta\Phi = \frac{16\pi^2\sqrt{2}G\eta_0}{\beta^{3/2}} I_{1/2}(\lambda e^{\beta\Phi_{eff}}), \quad (13)$$

and relating the Lagrange multipliers λ , β and Ω to the constraints M , E and \mathbf{L} . We stress that, for long-range systems, the mean-field approximation is *exact* in a suitable thermodynamic limit (here, $N \rightarrow +\infty$ with $\eta = \beta GM/R$ and $\Lambda = -ER/GM^2$ fixed) so that our “thermodynamical” approach is entirely rigorous and simpler than the “statistical” approach based on formal path integrals (e.g., Votyakov et al. 2002). The exactness of the mean-field approximation for long-range systems can be justified by the theory of large deviations in mathematics (Michel & Robert 1994). Note that if we fix β and G , the thermodynamic limit corresponds to $N \rightarrow +\infty$ with N/R fixed (de Vega & Sanchez 2002) but other combinations of the parameters can be considered (e.g., $G \sim 1/N$ for fixed β and R).

2.2. The box model

It is easy to see that Eq. (13) has no physical solution. Indeed, the density decreases as r^{-2} at large distances so that the total mass of the configuration is infinite in contradiction with our starting hypothesis. This means that there is no maximum entropy state in an unbounded domain. Therefore, the statistical mechanics of self-gravitating systems is essentially an out of equilibrium problem (see Chavanis 2003a for more details). In practice, the distribution function must be modified at high energies either because (i) the system is tidally truncated (e.g., globular clusters, dark matter halos) (ii) violent relaxation is incomplete (e.g., elliptical galaxies). An interesting (and astrophysically plausible) distribution function which takes into account both an external confinement and a small scale cut-off is given by (Chavanis 1998)

$$f = \eta_0 \frac{e^{-\beta\epsilon} - e^{-\beta\epsilon_m}}{\lambda + e^{-\beta\epsilon}}, \quad (14)$$

for $\epsilon \leq \epsilon_m$ and $f = 0$ for $\epsilon \geq \epsilon_m$ (where ϵ_m is the escape energy). This distribution function can be derived from a Fokker-Planck equation appropriate to self-gravitating fermions and it generalizes the Michie-King model for quantum particles (or collisionless stellar systems). This distribution function will be studied specifically in another paper. For the present, we shall keep the full Fermi-Dirac distribution function (10) and confine the system within a spherical box of radius R so as to avoid the infinite mass problem while preserving the rotational symmetry of the system.

2.3. Asymptotic limits $T = 0$ and $T \rightarrow +\infty$

It will be convenient in the following to work with dimensionless variables defined by

$$\mathbf{x} = \frac{\mathbf{r}}{R}, \quad n = \frac{\rho}{(M/R^3)}, \quad \phi = \frac{\Phi}{(GM/R)},$$

$$\Omega' = \Omega \left(\frac{R^3}{GM} \right)^{1/2}, \quad \mu = \eta_0 \sqrt{512\pi^4 G^3 M R^3}. \quad (15)$$

This is equivalent to setting $M = R = G = 1$ in the dimensional equations and we shall adopt this convention in the following. Then, the degeneracy parameter is given by $\mu = 16\sqrt{2}\pi^2\eta_0$. We also define $\psi = \beta\Phi$ and $\omega = \sqrt{\beta}\Omega$. Denoting by ψ_0 the value of ψ at $r = 0$ and introducing the uniformizing variable $k = \lambda e^{\psi_0}$, the Fermi-Poisson equation (13) becomes

$$\Delta\psi = \mu\sqrt{T}I_{1/2}(ke^{\psi-\psi_0-\frac{1}{2}\omega^2s^2}), \quad (16)$$

where $s = r \sin \theta$ denotes the distance to the axis of rotation. Eq. (16) must be solved with the condition $\psi \rightarrow 0$ at infinity. Before solving this equation in the general case, we first discuss important asymptotic limits.

For $k \rightarrow +\infty$, we can use the limiting form of the Fermi integral

$$I_n(t) \sim \frac{1}{t}\Gamma(n+1), \quad (t \rightarrow +\infty), \quad (17)$$

and we obtain the Boltzmann-Poisson equation

$$\Delta\psi = \frac{\mu\sqrt{\pi T}}{2k} e^{-\psi+\psi_0+\frac{1}{2}\omega^2s^2}, \quad (18)$$

for a rotating isothermal gas. This corresponds to the high temperature limit of the Fermi distribution. Indeed, for $T \rightarrow +\infty$ the distribution function (10) is Maxwellian

$$f = \frac{\eta_0}{\lambda} e^{-\beta(\frac{w^2}{2} + \Phi_{eff})}. \quad (19)$$

Alternatively, for $k \rightarrow 0$, we can use the limiting form of the Fermi integral

$$I_n(t) \sim \frac{(-\ln t)^{n+1}}{n+1}, \quad (t \rightarrow 0), \quad (20)$$

and obtain the Lane-Emden equation

$$\Delta\psi = \frac{2}{3}\mu\sqrt{T}(-\ln k - \psi + \psi_0 + \frac{1}{2}\omega^2s^2)^{3/2}, \quad (21)$$

for a rotating polytrope of index $n = 3/2$. This corresponds to the low temperature limit of the Fermi distribution in which the structure is completely degenerate. Indeed, for $T = 0$, the distribution function (10) is a step function

$$f = \eta_0 H(\epsilon_J - \epsilon_F), \quad (22)$$

where ϵ_J is the Jacobi energy, $\epsilon_F = -(1/\beta)\ln \lambda$ is the Fermi energy and H is the Heaviside function. Therefore, the Fermi-Dirac distribution function connects continuously isothermal and polytropic distributions for high and low temperatures.

2.4. Integral constraints

According to the classical work of James (1964), rotating polytropes with index $n > 0.808$ do not bifurcate to non-axisymmetric structures. At $T = 0$, the Fermi gas is equivalent to a polytrope of index $n = 3/2$ and so it does not bifurcate. We expect this property to persist at non-zero temperature since, at $T \neq 0$, we have essentially a polytrope $3/2$ surrounded by a dilute halo. Therefore, we shall restrict ourselves to axisymmetric solutions of Eq. (16). In that case, the angular momentum can be written $\mathbf{L} = I\Omega$ where I is the moment of inertia

$$I = 2\pi \int_{-1}^{+1} \int_0^1 \rho r^4 (1 - \mu^2) dr d\mu, \quad (23)$$

where $\mu = \cos \theta$.

The energy can be deduced from the Virial theorem

$$E = -K + \oint \mathbf{p} \cdot d\mathbf{S}. \quad (24)$$

The kinetic energy K incorporates a rotational contribution

$$K_{rot} = \frac{1}{2} \mathbf{L} \cdot \mathbf{\Omega} = \frac{1}{2} I\Omega^2, \quad (25)$$

and a thermal contribution

$$K_{th} = \frac{3}{2} \int p d^3 \mathbf{r}, \quad (26)$$

where $p = \frac{1}{3} \int f w^2 d^3 \mathbf{w}$ is the local pressure. Using Eq. (10), it can be put in the form

$$p = \frac{\mu}{6\pi} T^{5/2} I_{3/2} (k e^{\psi - \psi_0 - \frac{1}{2} \omega^2 s^2}). \quad (27)$$

2.5. A short description of the numerical procedure

Using the variables introduced previously, the Gauss theorem can be written as

$$\oint \nabla \psi \cdot d\mathbf{S} = \frac{4\pi}{T}, \quad (28)$$

where the surface integral is computed on the spherical box. Now, using the decomposition of the gravitational potential in normalized spherical harmonics, i.e.,

$$\psi = \sum_{l,m} \psi_{lm}(r) Y_{lm}(\theta, \phi), \quad (29)$$

it turns out that

$$T = \frac{4\pi}{\psi'_{00}(1)}. \quad (30)$$

Therefore, Eq. (16) depends only on three parameters μ , Ω and k . The degeneracy parameter μ and the angular velocity Ω specify a series of equilibria parametrized by the uniformizing variable k . Given these three parameters, the Fermi-Poisson equation (16) can be solved by an iterative procedure. For that purpose, the radial components of the potential, i.e. $\psi_{lm}(r)$, are discretized on the

Gauss-Lobatto grid which ensures spectral convergence. Typically, the resolution used for the following numerical results was 100 radial grid points and a decomposition on 16 spherical harmonics.

The temperature $T(\mu, \Omega, k)$, the energy $E(\mu, \Omega, k)$ and the angular momentum $L(\mu, \Omega, k)$ can then be determined by Eqs. (30), (24) and (23). It is then possible to compute the caloric curves $E(T)$ for given μ and Ω (or L) by eliminating k from the previous relations.

3. Caloric curve for low values of the degeneracy parameter (high cut-off)

We first describe the figures of equilibrium of the rotating self-gravitating Fermi gas for a degeneracy parameter $\mu = 100 \leq \mu_{MTP} = 2670$. For this value, the influence of the small-scale cut-off (played here by the exclusion principle) is strong in average and stabilizes the system with respect to the gravothermal catastrophe.

3.1. Non-rotating configurations

The caloric curve of non-rotating self-gravitating fermions has been discussed in a preceding paper (Chavanis 2002b) in both canonical and microcanonical ensembles and for arbitrary values of the degeneracy parameter μ . For non-rotating systems, the results obtained with fermions are similar to those obtained with other small-scale regularization, the small-scale cut-off playing the same role as the inverse of the degeneracy parameter (Stahl et al. 1994, Chavanis & Ispolatov 2002).

We first discuss the microcanonical ensemble corresponding to an isolated system with fixed energy. For $\mu < \mu_{MTP} = 2670$, there exists only one extremum of entropy for each energy and it is a *global* entropy maximum. The caloric curve is plotted in Fig. 1. For high energies, the density is almost homogeneous (Fig. 2g). This forms the “gaseous” phase. For energies close to the minimum accessible energy $E_{min} = -6.42 \cdot 10^{-2} \mu^{2/3}$, the temperature goes to zero and the system is completely degenerate (Fig. 2a). It has the same structure as a classical white dwarf star, i.e. a polytrope of index $n = 3/2$. This forms the “condensed” phase. For intermediate energies ($E_{cond} < E < E_{gas}$), corresponding to the region of negative specific heats $C = dE/dT < 0$, the system has a “core-halo” structure with a degenerate nucleus (fermion ball) and a dilute isothermal atmosphere (Fig. 2d). This is like a solid condensate embedded in a vapor in usual phase transitions. This “mixed phase” is intermediate between the pure condensed phase and the pure gaseous phase.

We now describe the canonical ensemble in which the temperature T is fixed instead of the energy E . We recall that, for self-gravitating systems, the validity of using the canonical ensemble to describe the statistics of a sub-system cannot be established from the microcanonical ensemble since energy is not additive (Padmanabhan 1990). Therefore, the notion of thermostat has to be defined carefully. The canonical ensemble can make sense

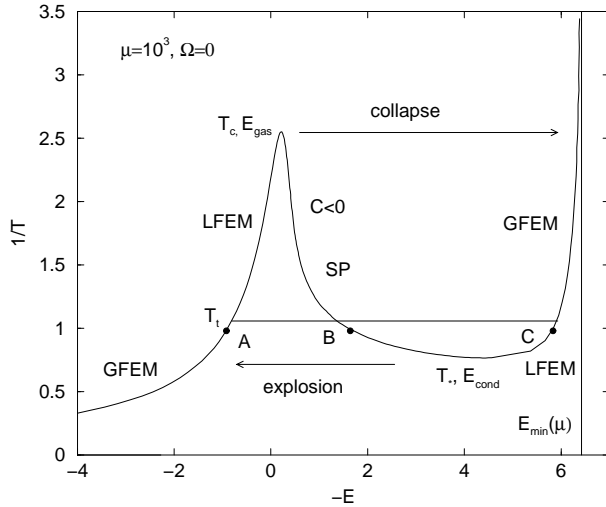


Fig. 1. The caloric curve for a non-rotating system with $\mu = 1000 < \mu_{MTP} = 2670$. In the microcanonical ensemble (fixed E), the system slowly evolves from the gaseous phase to the condensed phase, passing by a mixed phase, as energy decreases. In the canonical ensemble (fixed T), the system undergo a sharp phase transition at a critical temperature (see text). Below T_c , the gaseous states undergo a gravitational collapse (Jeans instability); above T_* , the condensed states undergo an explosion. Between, T_t and T_c (resp. T_*) the gaseous (resp. condensed) states are *metastable*. By varying the temperature of the system between T_* and T_c , we can generate an *hysteretic cycle* between the gaseous and the condensed phase.

if the system is in contact with a thermostat of a different nature (e.g., a radiation background) that imposes its temperature. In that case, the usual canonical ensemble interpretation holds. In the canonical ensemble, the region of negative specific heat is unstable as it corresponds to saddle points of free energy $J = S - \beta E$ (Katz 1978, Chavanis & Sommeria 1998). It is replaced by a canonical first order phase transition connecting the gaseous phase for $T > T_t(\mu)$ to the condensed phase for $T < T_t(\mu)$. Therefore, the mixed “core-halo” states with $C < 0$ are thermodynamically forbidden in the canonical ensemble. The gaseous states with temperature $T_c < T < T_t$ are metastable (local maxima of free energy) but they are long-lived. They can play an important role reminiscent of a supercooled state of the Van der Waals gas (in the limit $\mu \rightarrow +\infty$ for which $T_t \rightarrow +\infty$ they correspond to the *observed* structures). At $T < T_c$ they undergo a gravitational collapse (zeroth order phase transition) coinciding with Jeans instability criterion (Chavanis 2002e). The outcome of this collapse is the formation of a “fermion ball” containing almost *all* the mass. For $\mu \rightarrow +\infty$, the isothermal collapse leads to a Dirac peak (see Sec. 5). The condensed states with temperature $T_t < T < T_*$ are also metastable and long-lived (if they are initially prepared in such states). They will undergo an “explosion”, reversed to the collapse, if they are heated above T_* . This explo-

sion transforms the dense core into a relatively uniform mass distribution. By varying the temperature between T_* and T_c we can generate an *hysteretic cycle* in the canonical ensemble. This hysteresis cycle was first reported in Chavanis (2003b). Recently, it has been followed numerically with a simplified model of self-gravitating Brownian fermions (Chavanis, Ribot & Rosier 2003). More details on these phase transitions can be found in Chavanis (2002b). It is shown in particular that the first order canonical phase transition disappears for $\mu < \mu_{CTP} = 83$, i.e. for very high cut-off values. This is simply because the small-scale “repulsion” prevails over gravity.

3.2. Slowly rotating configurations

The slowly rotating configurations of an isothermal gas (possibly degenerate) can be determined semi-analytically by using perturbative expansions of the Boltzmann-Poisson or Fermi-Poisson equations in terms of the dimensionless rotation parameter $v = \Omega^2/2\pi G\rho_0$ (Chavanis 2002c). To lowest order in the expansion, the effect of rotation is just to flatten the system and to shift the onset of instability (see Sec. 5). For $T = 0$ (or $E = E_{min}$), we recover the distorted polytrope of index $n = 3/2$ studied by Milne (1923) and Chandrasekhar (1933). In the region of negative specific heats, this “rotating fermion ball” is surrounded by a gaseous halo. For high energies, the system is non degenerate. Therefore, the description of the equilibrium phase diagram is very similar to that of the non-rotating Fermi gas.

3.3. Spheroidal structures

For higher values of rotation, the flattening increases and the system takes a spheroidal structure. For $E \rightarrow E_{min}$, we have a rapidly rotating “fermion spheroid” (Fig. 2b). This structure is completely degenerate and highly concentrated. In particular, it is insensitive to the confining box. As energy increases further, the spheroid is only partially degenerate and extends to larger and larger distances (Fig. 2e). The rotation affects in priority the low density external region while the dense core of the configuration remains almost spherical. In the region of negative specific heats ($E_{cond} < E < E_{gas}$), the “spheroid” is surrounded by a diffuse halo. This corresponds to a mixed phase. This “spheroid-halo” structure generalizes the “core-halo” structure of non-rotating systems. For even larger values of energy, the spheroid would extend outside the box so that the system becomes almost one-dimensional and depends only on the axial coordinate z (Fig. 2h). Note, however, that the density contrast is extremely low ($\mathcal{R} = \rho(0)/\rho(R) \simeq 1.00022$) so that the structure is essentially homogeneous.

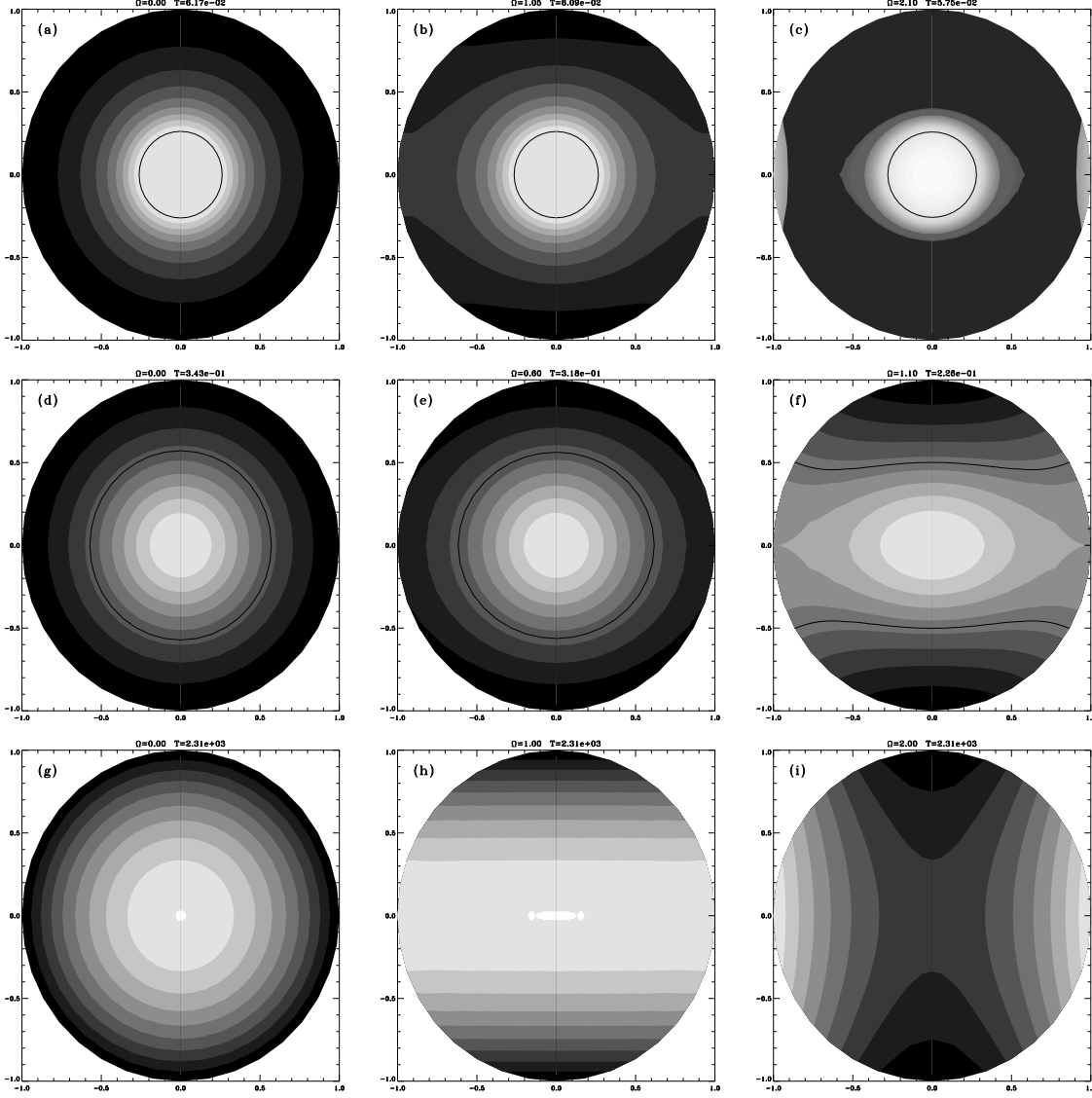


Fig. 2. Plot of the density (logarithmic scale) in a meridional section of the box. The solid line marks the level where density is 0.05, the central density being unity. The first row shows configurations at very low temperature/energy (condensed phase). The second row shows configurations in the region of negative specific heats (mixed phase). Such structures are forbidden (unstable) in the canonical ensemble. The third row shows configurations at high temperature/energy (gaseous phase). Alternatively, the first column corresponds to non-rotating systems, the second column to slowly rotating systems and the third column to systems rotating close to the Keplerian limit.

3.4. Keplerian limit

For $E = E_{min}$, the temperature drops to zero and the system is equivalent to a pure polytrope with index $n = 3/2$. The structure of rapidly rotating polytropes is well-known (James 1964). For rigid polytropes with index $n < 0.808$, the system is sensitive to non-axisymmetric instabilities of various forms. Therefore, at sufficiently high rotations, the spheroidal sequence bifurcates to more complicated structures (Chandrasekhar 1969). However, for $n > 0.808$, non-axisymmetric instabilities are inhibited and the series of equilibria has a different evolution. The polytrope develops a *cusp* at the equator at a point where the gravitational force balances the centrifugal force (Fig. 2c).

This is the so-called Keplerian (or break-up) limit corresponding to a critical angular velocity Ω_{max} such that $\Omega_{max}^2 R_e^3 = GM$, where R_e is the equatorial radius. There is no equilibrium state for $\Omega > \Omega_{max}$ as mass is ejected from the equatorial surface by the centrifugal force (mass shedding). The tendency to expel some mass far away may be related to the formation of a Keplerian disk above Ω_{max} . In that case, we must allow for differential rotation and this does not correspond to a statistical equilibrium state (for which, we recall, the angular velocity is constant). Mathematically, above Ω_{max} , the maximization problem leading to Eq. (10) has no solution that are everywhere differentiable. The formation of an equatorial cusp at $\Omega = \Omega_{max}$ marks the break-up of differentiability

and the complete change of structure. For $\Omega > \Omega_{max}$, the system may resemble a “cuspy condensate” + some matter accumulated at the box (ejected by the central body). We can also wonder whether non-axisymmetric structures can form above Ω_{max} . Indeed, there exists “double-cluster” solutions for polytropes with index $n > 0.808$ (Hachisu & Eriguchi 1984) but they bifurcate *discontinuously* from the spheroidal sequence. Therefore, they may be viewed as two local equilibrium states rather than a global one.

For $E = E_{min}$ and $\Omega = \Omega_{max}$, all the mass is in the cuspy polytrope. As E increases along the line of maximum rotation, the polytrope extends in size and is embedded in a disk-like halo (Fig. 2f). The maximum angular velocity $\Omega_{max}(E)$ decreases with E . This is because the size of the polytrope increases so that it is more easily affected by rotation. At high energies, the polytrope is very extended and the cusp would form outside the confining box. Therefore, the structure of the system is highly affected by the wall and this makes possible to achieve arbitrary large values of angular velocity. As a result, the maximum angular velocity increases with the energy when E is large. For high rotations and high energies, the matter accumulates on the wall due to the centrifugal force (Fig. 2i). The density profile is close to the law

$$\rho = A e^{\frac{1}{2} \beta \Omega^2 s^2}, \quad (31)$$

which corresponds to the density of a rotating gas without self-gravity. Note that the iso-density lines are axial so that a complete change of symmetry has occurred from Fig. 2h to Fig. 2i.

3.5. Equilibrium phase diagram

The caloric curve $T(E)$ is plotted in Fig. 3 for different values of angular velocity. It has the typical “N-shape” structure previously found for non-rotating and slowly rotating systems with high cut-off. The onset of instability can be determined by a turning point criterion (Katz 1978). For $\mu = 100$, the equilibrium states are always stable in the microcanonical ensemble (they are maxima of entropy at fixed mass, energy and angular momentum) but they are unstable in the canonical ensemble in the region of negative specific heats (they are saddle points of free energy at fixed mass, temperature and angular velocity). We see that, for moderate rotations, the structure of the caloric curve does not change dramatically with respect to the non-rotating case. It is just a natural continuation of previously reported results. However, at high rotations, the system is sensitive to mass shedding and there exists a maximum angular velocity Ω_{max} for each value of energy and temperature (Keplerian limit).

The phase diagram in the (E, Ω) plane is plotted in Fig. 4. Since the energy is assumed to be fixed, this diagram corresponds to the microcanonical description¹.

¹ We have used the angular velocity as a control parameter instead of the angular momentum for commodity but also because it is the most natural variable to characterize a rotating

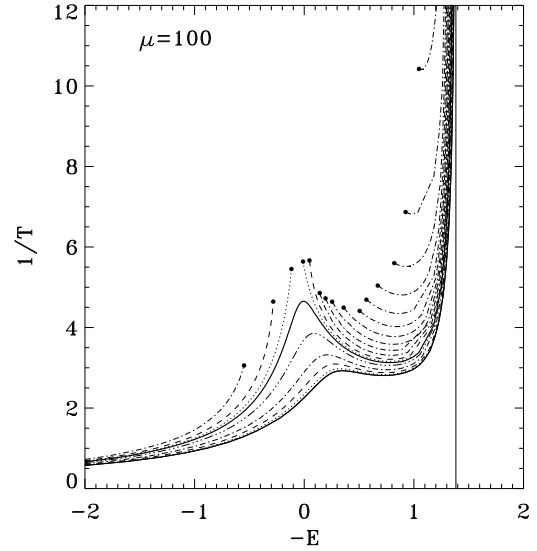


Fig. 3. The caloric curve of a rotating system with $\mu = 100$. It has a *N*-shape structure characteristic of self-gravitating systems with large cut-off ($\mu \leq \mu_{MTP} = 2670$). The “gaps” in energy and temperature at high rotations are due to the absence of uniformly rotating solution above the Keplerian limit.

In continuity with the non-rotating case, the horizontal structure of the diagram consists of three regions: a pure “condensed” phase for $E < E_{cond}$, a pure “gaseous” phase for $E > E_{gas}$ and a mixed “core-halo” phase for intermediate energies. Vertically, the diagram proceeds with increasing flattening until the Keplerian limit is reached for $\Omega = \Omega_{max}(E)$. Above this line, the system is expected to expulse matter far away and, possibly, create a Keplerian disk or break into fragments.

The phase diagram in the (T, Ω) plane is plotted in Fig. 5. Since the temperature is assumed to be fixed, this diagram corresponds to the canonical description. The mixed phase with negative specific heats allowed in the microcanonical ensemble is replaced by a phase transition connecting the “gaseous” phase to the “condensed” phase. Between T_c and T_* the system can be in a metastable state. If it is initially prepared in a gaseous state, it will remain gaseous until the minimum temperature T_c at which it will collapse and become condensed. Inversely, if the system is initially prepared in a condensed state, it will remain condensed until the maximum temperature T_* at which it will explode and become gaseous (see Fig. 1). Therefore, the configuration of the system in the H -zone

system. Indeed, the conservation of angular momentum should not be taken in a strict sense because it can always be satisfied by ejecting a small amount of mass far away with weak influence on the other constraints. For similar remarks concerning the role of angular momentum in the context of vortex dynamics, see Brands et al. (1999).

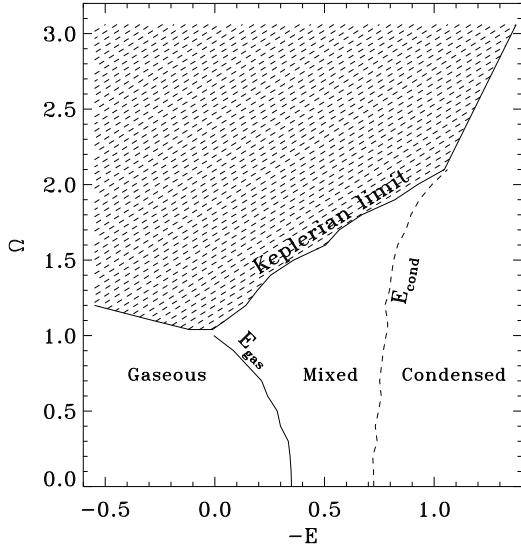


Fig. 4. Microcanonical phase diagram in the (E, Ω) plane for $\mu = 100$. The maximum angular velocity $\Omega_{max}(E)$ depends on the energy. It is maximum for the $T = 0$ configuration (which corresponds to a $n = 3/2$ polytrope). The parameters of this terminal point are $\Omega_{max} = 3.06$ and $E_{min} = -1.37$.

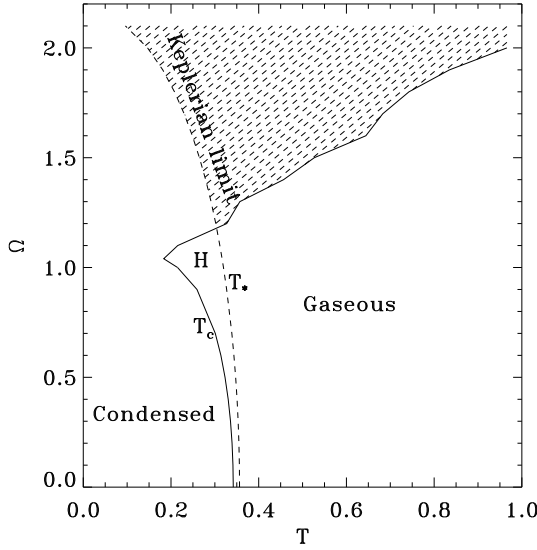


Fig. 5. Canonical phase diagram in the (T, Ω) plane for $\mu = 100$. The H -zone corresponds to an hysteretic zone where the actual phase depends on the history of the system.

depends on its history. This is like a hysteretic cycle in magnetism.

4. Caloric curve for high values of the degeneracy parameter (low cut-off)

We now consider the case of a high value of the degeneracy parameter $\mu = 10^5 > \mu_{MTP} = 2670$ so that the influence of the small-scale cut-off is weaker in average and the conditions required to set up a gravothermal catastrophe are fulfilled.

The caloric curve $T(E)$ is plotted in Fig. 6 for different values of angular velocity. It has the typical “Z-shape” structure (resembling a “dinosaur’s neck”) previously found for non-rotating or slowly rotating systems (Chavanis & Sommeria 1998, Chavanis 2002b,c). The upper branch corresponds to non-degenerate states (gaseous phase) and the lower branch corresponds to core-halo states (condensed phase). A first order *microcanonical* phase transition is expected to occur at $E_t(\mu)$ since at this energy the two phases have the same entropy (Fig. 7). However, the first order phase transition may not take place in practice because the gaseous states with energy $E_c < E < E_t$ are metastable (local entropy maxima) and long-lived (Katz & Okamoto 2000, Chavanis & Ispolatov 2002). The collapse (gravothermal catastrophe) will set in at, or near, the critical energy E_c (Antonov energy) at which the gaseous phase disappears. This corresponds to a zeroth order microcanonical phase transition accompanied by a discontinuity of temperature and entropy. The collapse stops when the central region becomes degenerate and forms a dense nucleus. The resulting configuration has a “core-halo” structure. Contrary to the canonical situation, the nucleus contains only a *moderate* fraction of mass. For $\mu \rightarrow +\infty$, it reduces to a single binary (see Sec. 5). The rest of the mass is diluted in a hot envelop that is held by the walls of the box. For an open system, the halo would be dispersed at infinity so that only the degenerate nucleus would remain. This behaviour, with the expulsion of an envelope, is more consistent with the process of white dwarf formation than a complete collapse of the system at fixed T . This is an astrophysical evidence that the microcanonical ensemble is more appropriate than the canonical one. The condensed states with energy $E_t < E < E_*$ are also metastable and long-lived. An “explosion”, reversed to the gravothermal catastrophe, will occur above E_* if the system is initially prepared in the condensed phase (see Fig. 7). By varying the energy between E_* and E_c we can generate an *hysteretic cycle* in the microcanonical ensemble (Chavanis 2003b).

The phase diagram describing the microcanonical phase transition is represented in Fig. 8. It can be compared with the phase diagram describing the canonical phase transition for $\mu = 100$ (see Fig. 5), the role of energy E and temperature T being reversed. In particular, there exists a H -zone in which the structure of the system (gas or condensate) depends on its history. For smaller energies ($E < E_c$), the system is in a mixed phase with negative specific heats. For even lower energies $E_{cond} \sim -117$ (not represented on the diagram), we leave the region of negative specific heats and enter the pure condensed phase

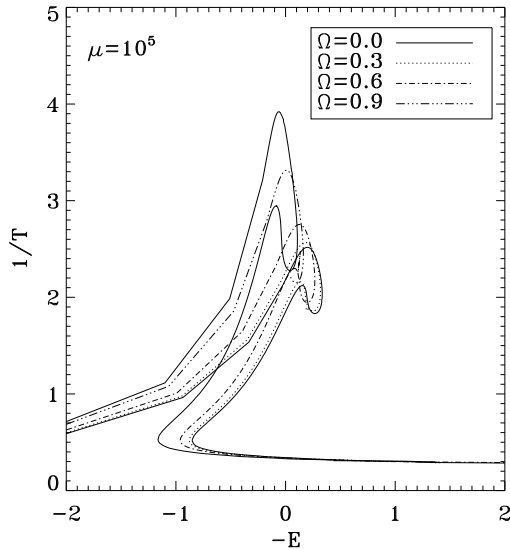


Fig. 6. The caloric curve of a rotating system with $\mu = 10^5$. It has a Z-shape structure (dinosaur's neck) characteristic of self-gravitating systems with small cut-off ($\mu \geq \mu_{MTP} = 2670$).

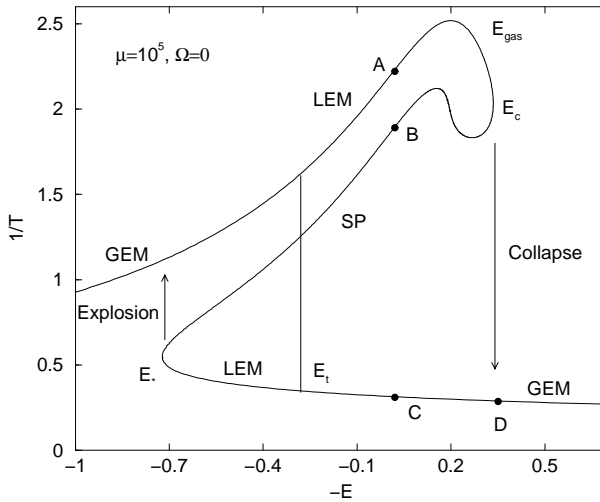


Fig. 7. Caloric curve of a self-gravitating system with $\mu = 10^5$ (here $\Omega = 0$). Between E_t and E_c (resp. E_*) the gaseous states (resp. condensed states) are *metastable*. A collapse occurs at E_c (gravothermal catastrophe) and an explosion occurs at E_* . By varying the energy of the system between E_* and E_c , we can generate an hysteretic cycle in the microcanonical ensemble.

as in Fig. 4. More details on these phase transitions can be found in Chavanis (2002b). It is shown in particular that the microcanonical first order phase transition disappears for $\mu < \mu_{MTP} = 2670$.

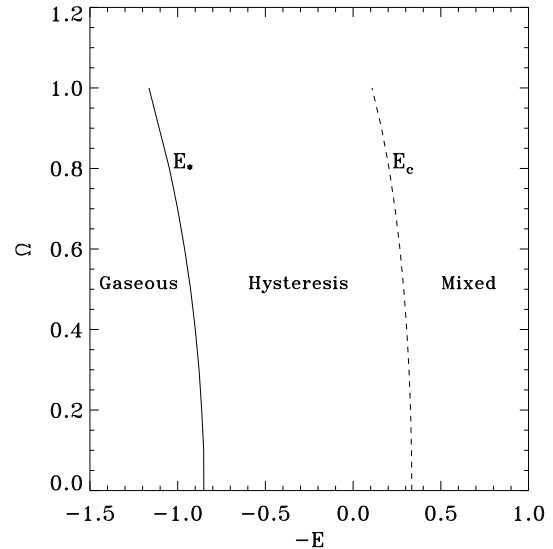


Fig. 8. Microcanonical phase diagram for $\mu = 10^5$. The H -zone corresponds to an hysteretic zone where the actual phase depends on the history of the system.

5. Gravothermal catastrophe for classical self-gravitating particles

We now consider the limit $\mu \rightarrow +\infty$ corresponding to classical particles. In that limit, the particles do not feel any kind of exclusion or small-scale cut-off. This is the situation relevant for globular clusters.

In the non degenerate limit, the caloric curve has a classical spiral shape (Fig. 9). We recall that, in the absence of small-scale cut-off, the equilibrium states are only metastable as they correspond to *local* maxima of the thermodynamical potential (entropy or free energy). These metastable states play however an important role as they correspond to the observed structures (see discussion in Chavanis 2003a). In the microcanonical ensemble, the gravothermal catastrophe sets in at the Antonov energy E_c . The microcanonical phase diagram in (E, Ω) plane is drawn in Fig. 10 and shows in particular the evolution of the Antonov critical energy $E_c(\Omega)$ with the rotation. The critical energy $E_c(\Omega)$ increases with rotation so that gravitational collapse occurs *sooner* than in the non-rotating case. This confirms the results of the perturbative approach (Chavanis 2002c). Qualitatively, the critical energy increases due to the rotational term $\frac{1}{2}I\Omega^2$ in the energy (see Sec. 2.4). The result of the collapse is to form a *binary* with large binding energy. Since total energy is conserved, the gravitational energy released by the binary is redistributed in a dilute halo in the form of thermal energy. This evolution is natural in the microcanonical ensemble since it can produce very high (ideally diverging) values of entropy due to the divergence of the temperature. It is also vindicated by numerical simulations of the orbit averaged Fokker-Planck equation or fluid equations (Cohn 1980, Lynden-Bell & Eggleton 1980). These simulations

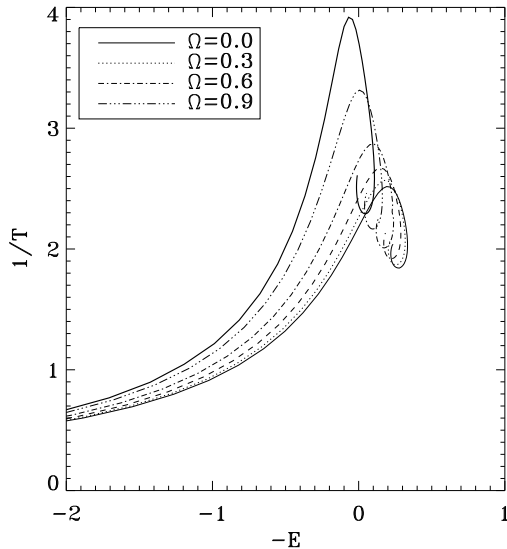


Fig. 9. Caloric curves corresponding to classical point masses ($\mu \rightarrow +\infty$) for different values of the angular velocity. The thick line is for $\Omega = 1$. Below E_c , the gravothermal catastrophe leads to the formation of a binary (microcanonical ensemble). Below T_c , the isothermal collapse generates a Dirac peak (canonical ensemble).

show that the collapse of globular clusters is self-similar and leads to a finite time singularity with a density profile $\rho \sim r^{-\alpha}$ with $\alpha \simeq 2.2$. The mass contained in the core goes to zero (indicating that the collapse is halted by the formation of binaries) while the central temperature raises to $+\infty$ since $\alpha > 2$.

In the canonical ensemble, the collapse sets in at the critical temperature T_c . The evolution of this critical temperature with the angular velocity is represented in Fig. 10. It is found that $T_c(\Omega)$ decreases with Ω so that gravitational collapse is *delayed* in the canonical ensemble. This corroborates the results found with the perturbative approach (Chavanis 2002c). The result of the collapse is to form a *Dirac peak*, i.e. a state where all the mass is concentrated at the center. This evolution is natural in the canonical ensemble since it can produce very high (in fact diverging) values of free energy $J = S - \beta E$ due to the divergence of the potential energy. This isothermal collapse can be followed dynamically with the Navier-Stokes equations for a gaseous system with an equation of state $p = \rho T$ where T is fixed (Penston 1969). It can also be studied with a simple dynamical model of self-gravitating Brownian particles in a canonical description (Chavanis et al. 2002). In this model, there is first a finite time singularity leading to a r^{-2} density profile. Then, the collapse continues after the singularity is formed and the Dirac peak appears in the post-collapse regime due to the accretion of mass (Sire & Chavanis 2002). We expect this two-stage behaviour to persist in the case of more relevant dynamical models. This is an important point for numerical simulations in

cosmology because if we only consider the first regime we conclude that the core contains no mass (while its density is high and scales as r^{-2}). However, in a post-collapse regime, a Dirac peak is formed which contains a macroscopic mass at a single point. We can wonder whether this mechanism (apparently not reported before) is related to the existence of black holes at the center of galaxies. In reality, small-scale cut-offs must be introduced (e.g. quantum degeneracy) and the black hole singularity is replaced by a “fermion ball” with a high mass. Note that in the microcanonical ensemble, there is no black hole singularity for classical point masses (the Dirac peak is replaced by a binary). Interestingly, for self-gravitating fermions, the condensate (fermion ball) contains a moderate but *macroscopic* fraction of mass (Chavanis & Sommeria 1998). This may explain the formation of massive objects at the center of galaxies in a microcanonical framework. The microcanonical description is the most relevant as it accounts for the transfers of energy between the core and the halo contrary to $T = 0$ models.

The divergence of entropy in the microcanonical ensemble due to the formation of a binary embedded in a halo is implicit in the work of Antonov (1962). It is also clear from the arguments given by Padmanabhan (1990) to show that the density of state diverges as we approach two particles to each other. The divergence of free energy in the canonical ensemble by forming a Dirac peak has been shown rigorously by Kiessling (1989) and heuristically by Chavanis (2002e). The inequivalence of statistical ensembles regarding the formations of binaries or Dirac peaks is further discussed in Appendix A and B of Sire & Chavanis (2002) for different space dimension D . In this approach, a family of distributions functions is constructed which provokes the explosion of entropy or free energy when a physical parameter is varied. These results can also be obtained by considering the small cut-off limit ($\mu \rightarrow +\infty$) of an analytical model of phase transitions (Chavanis 2002b).

6. Phase diagram of non-rotating systems

In previous sections, we have presented the equilibrium phase diagram of self-gravitating fermions as a function of the angular velocity Ω for a fixed degeneracy parameter μ . We shall now discuss the equilibrium phase diagram of self-gravitating fermions (or hard sphere systems) as a function of μ for $\Omega = 0$. These phase diagrams have not been published before.

The deformation of the caloric curve $T(E)$ as a function of the degeneracy parameter μ is described in Chavanis (2002b). This work completes earlier studies on phase transitions in self-gravitating systems by showing the small cut-off limit, characterized by an unwound spiral, leading to a first order microcanonical phase transition (earlier work essentially described the canonical first order phase transition). Typical curves illustrating first order canonical and first order microcanonical phase transitions are shown in Figs. 1 and 7. The equilibrium phase dia-

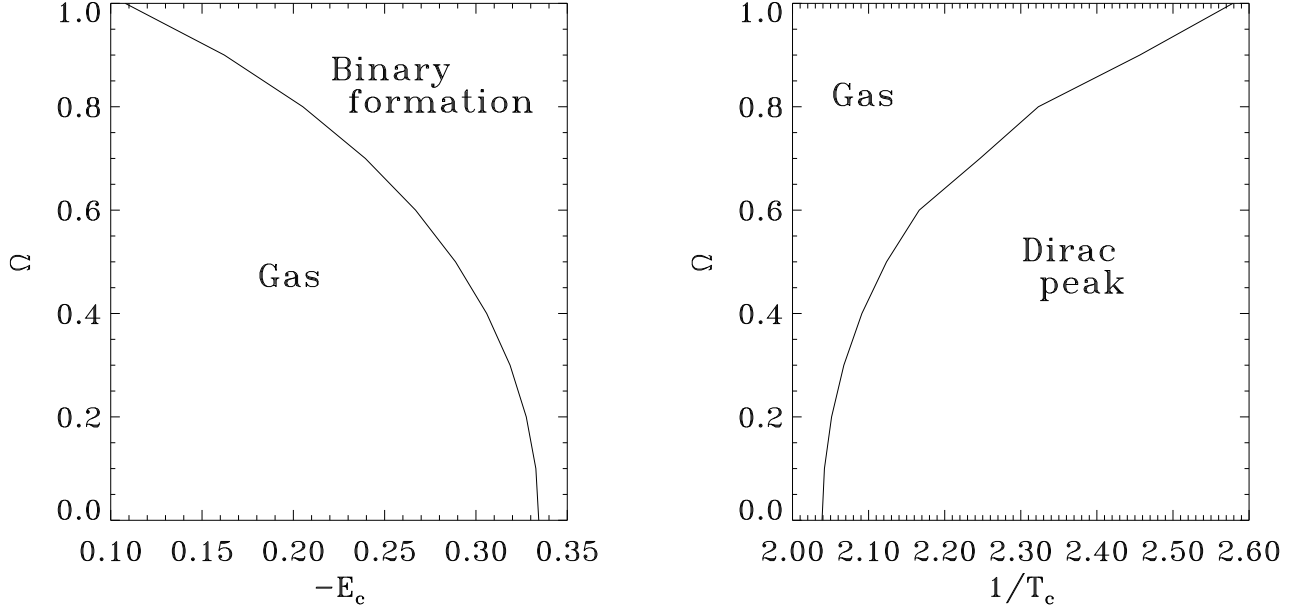


Fig. 10. Dependence of the Antonov critical energy and critical temperature with rotation. For high energies or high temperatures, the system is in a gaseous (metastable) phase. Below a critical energy or temperature, it enters the collapsed phase. In the microcanonical ensemble (fixed E), the collapsed state is made of a single binary (or a small group of stars) surrounded by a hot dilute halo. In the canonical ensemble (fixed T), the collapsed state is a Dirac peak. This Dirac peak forms in the post-collapse regime of the dynamical evolution.

gram of self-gravitating fermions can be directly deduced from these results by identifying characteristic energies and temperatures. In the canonical ensemble, we note T_t the temperature of transition (determined by the equality of the free energies of the two phases), T_c the end point of the metastable gaseous phase (first turning point of temperature) and T_* the end point of the metastable condensed phase (last turning point of temperature). The temperature of transition T_t is determined by a Maxwell construction (Chavanis 2003b). The canonical phase diagram is shown in Fig. 11. It shows in particular the canonical critical point $\mu_{CTP} = 83$ at which the canonical first order phase transition disappears and is replaced by a localized second order phase transition.

In the microcanonical ensemble, we note E_t the temperature of transition (determined by the equality of the entropy of the two phases), E_c (Antonov energy) the end point of the metastable gaseous phase (first turning point of energy) and E_* the end point of the metastable condensed phase (last turning point of energy). The energy of transition E_t is determined by a less standard Maxwell construction (Chavanis 2003b). We also denote by E_{gas} the energy at which we enter in the mixed phase with negative specific heat (first turning point of temperature) and E_{cond} the energy at which we leave the mixed phase and enter the condensed phase (last turning point of temperature). We also introduce the minimum energy E_{min} . The microcanonical phase diagram is shown in Fig. 12. It shows in particular the microcanonical critical point

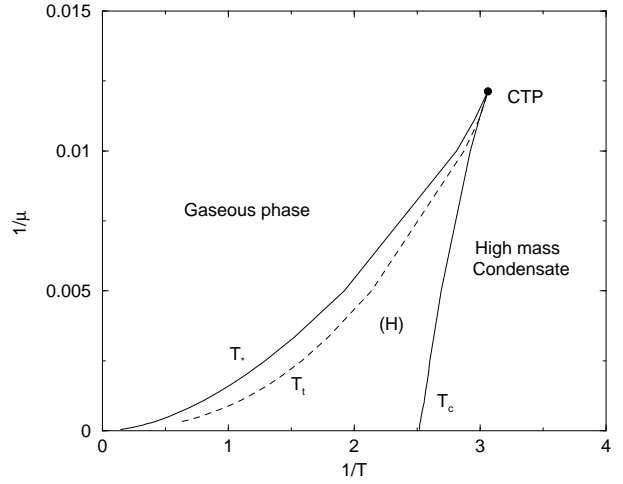


Fig. 11. Canonical phase diagram in (T, μ) plane for $\Omega = 0$. The H -zone corresponds to an hysteretic zone where the actual phase depends on the history of the system.

$\mu_{MTP} = 2670$ at which the microcanonical first order phase transition disappears. The structure of the equilibrium phase diagrams can be easily understood in the light of the preceding discussion (see Chavanis 2002b for more details). We note that the microcanonical phase diagram is more complex than the canonical one due to the existence of a negative specific region. Hence, the microcanonical ensemble is richer than the canonical one, as is well-known.

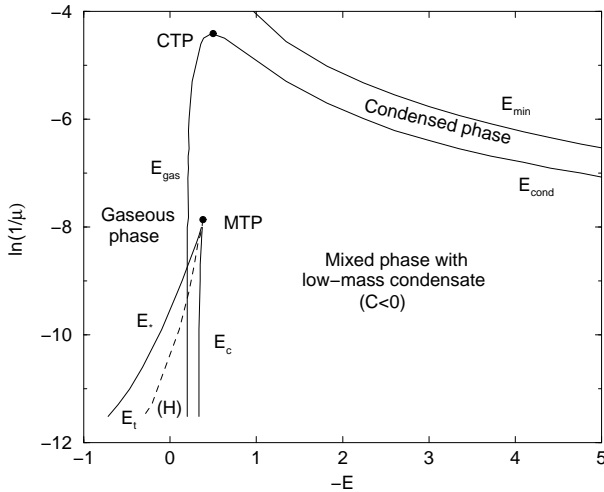


Fig. 12. Microcanonical phase diagram in (E, μ) plane for $\Omega = 0$. The phase diagram in MCE is more complex than in CE due to the existence of the negative specific heat region that is forbidden in CE.

7. Conclusion

We have calculated the statistical equilibrium states of self-gravitating fermions for arbitrary values of rotation and temperature (or energy). The divergence of the gravitational potential as $r \rightarrow 0$ has been avoided by considering quantum effects. This small-scale regularization is a physical one because the Pauli exclusion principle is a fundamental concept and fermionic matter is relevant in astrophysics. Isothermal and polytropic configurations (with index $n = 3/2$) are obtained as particular limits of our model ($T \rightarrow +\infty$ and $T = 0$). On the other hand, depending on the importance of rotation, we have obtained different types of structures such as fermion balls, fermion spheroids and cuspy structures. In the mixed phase, these condensed objects are surrounded by a diffuse isothermal halo. Clearly, the main drawback of our study is the necessity to enclose the system within an artificial box so as to prevent its complete evaporation (which is the true statistical equilibrium state for self-gravitating systems). A future extension of our study is to consider more realistic truncated models in order to avoid the artifice of a material box and take into account incomplete relaxation or tidal effects. We note, in passing, that the distribution function predicted by statistical mechanics cannot account for the triaxial structure of elliptical galaxies since no bifurcation from axisymmetric (spheroidal) to non-axisymmetric (ellipsoidal) structures are expected for uniformly rotating compressible bodies. The distribution function must depend on isolated integrals different from the single Jacobi integral (Contopoulos 1960). This is clearly a manifestation of incomplete relaxation but the construction of such isolated integrals is a highly complicated task and demands a very delicate analysis of the process of formation of elliptical galaxies.

We emphasize that the nature of the small-scale cut-off is of considerable importance for rotating objects because it can generate or inhibit non-axisymmetric instabilities. For example, the ordinary Fermi-Dirac distribution used in this paper and the model of Votyakov et al. (2002) have the same high temperature limit (an isothermal gas with $p = \rho T$) but a different low temperature limit. The Fermi gas at $T = 0$ corresponds to the equation of state $p = K \rho^{5/3}$ (polytropic core). The equation of state corresponding to a Fermi-Dirac distribution in configuration space $\rho = \rho_{\text{max}} / [1 + \lambda \exp(\beta \Phi_{\text{eff}})]$ is $p = T \ln(1 - \rho / \rho_{\text{max}})$, as can be obtained from the condition of hydrostatic equilibrium, and it leads to $\rho \rightarrow \rho_{\text{max}}$ as $T \rightarrow 0$ (solid core). In the former case, there is no bifurcation to non-axisymmetric structures at high rotations (at least in continuity with the spheroidal sequence) while such bifurcations occur in the latter. It is surprising that the equation of state corresponding to the model of Votyakov et al. (2002) does not coincide with the Van der Waals equation of state since they treat their system as a hard sphere gas. This may unveil a weakness in their counting analysis which is not standard and does *not* correspond to Lynden-Bell's statistics unlike their claim². It is also surprising that they do not obtain a richer variety of structures (at least in the low temperature regime) since rotating homogeneous bodies possess a rich bifurcation diagram as investigated since the 19-th century (Chandrasekhar 1969). These remarks show that the small-scale regularization must be given precise consideration depending on the situation contemplated.

The self-gravitating Fermi gas has several astrophysical applications: (i) Lynden-Bell's type of degeneracy may be relevant for galactic nuclei and dark matter (Lynden-Bell 1967, Kull et al. 1996, Chavanis & Sommeria 1998). (ii) Pauli's exclusion principle is relevant for white dwarfs and neutron stars (Chandrasekhar 1942, Hertel & Thirring 1971). In that context, the Fermi gas at non-zero temperature provides a simple theoretical model describing a phase transition from a “gaseous star” (for $T > T_c$) to a white dwarf or a neutron star (for $T < T_c$). To obtain a better description of these objects, special relativity must be taken into account for white dwarf stars (Chandrasekhar 1931) and general relativity is required in the case of neutron stars (Oppenheimer & Volkoff

² Although the Fermi-Dirac distribution in configuration space is subject to criticism in the case of self-gravitating systems, it is however the correct form of statistics for two-dimensional vortices (see Chavanis 2002a for a review on the analogy between stellar systems and 2D vortices). In that respect, it may be relevant to mention the work of Chen & Cross (1996) who found “two-vortex” equilibrium solutions in a circular domain when the conservation of angular momentum is accounted for. This can be viewed as the 2D version of the “double-star” structure found by Votyakov et al. (2002). Note that the presence of a confining box is crucial to maintain the double-vortex solution. Concerning the double-star structure, it is difficult to evaluate the influence of the artificial box in the work of Votyakov et al. (2002).

1939). (iii) It has been proposed recently that dark matter could be made of a collisionless gas of massive neutrinos. Therefore, the relevant distribution function is again the Fermi-Dirac distribution (Chavanis 2002f). The degeneracy is due either to the Liouville theorem (in the context of violent relaxation) or to Pauli's exclusion principle (if quantum effects are relevant). By cooling below a critical temperature, this neutrino gas is expected to undergo a phase transition to a compact object called a "fermion ball". It has been proposed that fermion balls could provide an alternative to black holes at the center of galaxies (Bilic & Viollier 1997). (iv) Incidentally, our study can also be connected to models of rotating stars (e.g., Roxburgh et al. 1965). Low mass stars ($M \lesssim 1.5 M_{\odot}$) of the main sequence have a radiative core and a convective envelope. Massive stars ($M > 1.8 M_{\odot}$) have the opposite configuration. Now, the convective region corresponds to a polytrope of index $n = 3/2$. Coincidentally, this case is precisely covered by our study.

On the other hand, hard spheres models have less direct applications in astrophysics because the inter-particle distance is always considerably larger than their size. Indeed, globular clusters can be either in dilute metastable equilibrium states (Michie 1963, King 1966) or in a collapsing phase ending up with the formation of binaries (Hénon 1961). These binaries can release sufficient energy to drive a re-expansion of the system (Inagaki & Lynden-Bell 1983, Bettwieser & Sugimoto 1984) so that complete collapse is prevented in practice. In each case, the size of the stars does not matter. The size of the atoms in stars does not matter neither because radiative transfers keep the star in a gaseous phase far from condensation. When a star collapses, gravity is balanced by quantum pressure not by the pressure of a hard sphere gas. In that respect, it may be useful to recall that the hard sphere model of Aronson & Hansen (1972) was presented as a crude model for neutron stars where the hard spheres were introduced to mimick quantum degeneracy. The hard-sphere model can however find physical applications in the context of planet formation resulting from the gravitational collapse of planetesimals in the solar nebula (Stahl et al. 1994, Chavanis 2000). However, the importance of rotation is expected to be weak and its main effect is just to flatten the planet.

Finally, our study has a direct relevance in terms of fundamental statistical mechanics. Indeed, the different types of phase transitions arising in the self-gravitating Fermi gas (Chavanis 2002b) have a very rich structure (inequivalence of statistical ensembles, negative specific heats, convex intruder in the entropy-energy curve, canonical and microcanonical first order phase transitions, second order phase transition, zeroth order phase transition, canonical and microcanonical critical points, metastable states, hysteretic cycle,...). Such properties are probably common to other systems with long-range interactions. In fact, the self-gravitating Fermi gas forms a generic example of systems displaying codimensions 0 and 1 singularities in the classification of phase transitions (for long-

range systems) recently proposed by Bouchet & Barré (2003).

References

Antonov, V.A. 1962, *Vest. Leningr. Gos. Univ.*, 7, 135
 Aronson, E.B. & Hansen, C.J. 1972, *ApJ*, 177, 145
 Bouchet, F. & Barré, J. 2003, submitted to *J. Stat. Phys.*
 Bettwieser, E. & Sugimoto, D. 1984, *MNRAS*, 208, 493
 Bilic, N. & Viollier, R.D. 1997, *Phys. Lett. B*, 408, 75
 Binney, J., Tremaine, S. 1987, *Galactic Dynamics* (Princeton Series in Astrophysics)
 Bonnor, W.B. 1956, *MNRAS*, 116, 351
 Boss, A.P. 1986, *Icarus*, 66, 330
 Boss, A.P. 1988, *Comm. Astrophys.*, 12, 169
 Brands, H., Chavanis, P.H., Pasmanter, R., Sommeria, J., 1999, *Phys. Fluids*, 11, 3465
 Chandrasekhar, S. 1931, *ApJ*, 74, 81
 Chandrasekhar, S. 1933, *MNRAS*, 93, 390
 Chandrasekhar S. 1942, *An Introduction to the Theory of Stellar Structure* (Dover)
 Chandrasekhar, S. 1969, *Ellipsoidal figures of equilibrium* (Yale University Press, New Haven)
 Chavanis, P.H. 1998, *MNRAS*, 300, 981
 Chavanis, P.H. 2000, *A&A*, 356, 1089
 Chavanis, P.H., 2002a, in: *Dynamics and thermodynamics of systems with long range interactions*, edited by Dauxois, T, Ruffo, S., Arimondo, E. and Wilkens, M. (Lecture Notes in Physics, Springer) [cond-mat/0212223]
 Chavanis, P.H. 2002b, *PRE*, 65, 056123
 Chavanis, P.H., 2002c, *A&A*, 396, 315
 Chavanis, P.H., 2002d, in: *Proceedings of the Conference on Multiscale Problems in Science and Technology*, edited by Antonic, N., van Duijn, C.J., Jäger, W. and Rikelic, A. (Springer, Berlin) [astro-ph/0212205]
 Chavanis, P.H., 2002e, *A&A*, 381, 340
 Chavanis, P.H., 2002f, in: *Proceedings of the Fourth International Heidelberg Conference on Dark Matter in Astro and Particle Physics*, edited by Klapdor-Kleingrothaus, H.V. (Springer, New-York) [astro-ph/0205426]
 Chavanis, P.H., 2003a, *A&A* in press [astro-ph/0207080]
 Chavanis, P.H., 2003b, in: *Proceedings of the TH-2002 conference on Theoretical Physics*, edited by Zinn-Justin, J., Iagolnitzer, D. and Rivasseau, V. (*Annales Henri Poincaré* and CD-rom)
 Chavanis, P.H., 2003c, submitted to *PRE* [cond-mat/0209096]
 Chavanis, P.H. & Ispolatov, I., 2002, *PRE*, 66, 036109
 Chavanis, P.H., Ribot, M. & Rosier, C. 2003, in preparation
 Chavanis, P.H., Rosier, C. & Sire, C., 2002, *PRE*, 66, 036105
 Chavanis, P.H. & Sommeria, J. 1998, *MNRAS*, 296, 569
 Chen, P. & Cross, M.C. 1996, *PRE*, 53, R3032
 Cohn, H., 1980, *ApJ*, 242, 765
 Contopoulos, G., 1960, *Z. Astrophys.*, 49, 273
 de Vega, H.J. & Sanchez, N. 2002, *Nucl. Phys. B*, 625, 409
 Emden, R. 1907, *Gaskugeln* (Teubner Verlag, Leipzig)
 Fowler, R.H. 1926, *MNRAS*, 87, 114
 Hachisu, I. & Eriguchi, Y. 1984, *PASJ*, 36, 239
 Hénon, M. 1961, *Ann. Astrophys.* 5, 369
 Hertel, P. & Thirring, W. 1971, in: *Quanten und Felder*, edited by H.P. Dürr (Vieweg, Braunschweig)
 Hjorth, J. & Madsen, J. 1993, *MNRAS* 265, 237
 Inagaki, S. & Lynden-Bell, D. 1983, *MNRAS* 205, 913

Ipser, J.R. & Horwitz G. 1979, *ApJ* 232, 863
 James, R.A. 1964, *ApJ* 140, 552
 Kandrup, H. 1981, *ApJ* 244, 316
 Katz, J. 1978, *MNRAS* 183, 765
 Katz, J. & Okamoto, I. 2000, *MNRAS* 371, 163
 Kiessling, M. 1989, *J. Stat. Phys.* 55, 203
 King, I.R. 1966, *ApJ* 71, 64
 Kull, A., Treumann, R.A., Böringer, H. 1996, *ApJ* 466, L1
 Lagoute, C. & Longaretti, P.Y. 1996, *A&A*, 308, 441
 Lynden-Bell, D. 1967, *MNRAS* 136, 101
 Lynden-Bell, D. & Eggleton, P.P. 1980, *MNRAS*, 191, 483
 Lynden-Bell, D. & Wood, R. 1968, *MNRAS*, 138, 495
 Michel, J., Robert, R. 1994, *Commun. Math. Phys.*, 159, 195
 Michie, R.W. 1963, *MNRAS*, 125, 127
 Milne, E.A. 1923, *MNRAS*, 83, 118
 Ogorodnikov, K.F. 1965, *Dynamics of stellar systems* (Pergamon)
 Oppenheimer, J.R. & Volkoff, G.M. 1939, *Phys. Rev.*, 55, 374
 Padmanabhan, T. 1990, *Phys. Rep.*, 188, 285
 Penston, M.V. 1969, *MNRAS*, 144, 425
 Roxburgh, I.W., Griffith, J.S. & Sweet, P.A. 1964, *Z. Astrophys.*, 61, 203
 Sire, C. & Chavanis, P.H. 2002, *PRE* 66, 046133
 Stahl, B., Kiessling, M.K.H. & Schindler, K. 1994, *Planet. Space Sci.* 43, 271
 Tremaine, S., Hénon, M. & Lynden-Bell, D. 1987, *MNRAS*, 227, 543
 Votyakov, E.V., Hidmi, H.I., De Martino, A. & Gross, D.H.E. 2002, *PRL*, 89, 031101